Journal of Materials Chemistry C

PAPER

View Article Online
View Journal | View Issue

Cite this: J. Mater. Chem. C, 2016, 4, 6907

Single-step synthesis of hyperbranched, luminescent Mn^{2+}-doped $ZnSe_{1-x}S_x$ nanocrystals using dichalcogenide precursors†

Mohammad S. Yazdanparast, Matthew T. Webb and Emily J. McLaurin*

Received 22nd March 2016,
Accepted 15th June 2016

DOI: 10.1039/c6tc01207h

www.rsc.org/MaterialsC

Taking advantage of dichalcogenide precursors, a simple, single-step heat-up method for obtaining Mn^{2+}-doped $ZnSe_{1-x}S_x$ nanocrystals (NCs) is presented. Tuning the ratios of diselendide and disulfide precursors results in alloys with varying shape, size and composition. When diphenyldiselenide (Ph_2Se_2) is used, highly branched networks of small NCs form. Dimethydisulfide (Me_2S_2) induces formation of larger NCs with less branching. Mixtures of the two exhibit branching proportional to the amount of Ph_2Se_2 *vs.* Me_2S_2, allowing formation of a series of branched Mn^{2+}-doped NCs. Interestingly, these NCs exhibit photoluminescence (PL) characteristic of Mn^{2+}, despite the large number of defects and unusual shapes they possess. This demonstrates Mn^{2+} can be successfully doped into NCs with several degrees of branching, in which it acts as an efficient radiative trap. Addition of thiol to the NCs led to a large enhancement in the Mn^{2+} PL. In organic solution, the sensitivity to thiol varied with the degree of NC branching, with hyperbranching NCs giving the most sensitive response. After transfer to aqueous solution, the Mn^{2+} PL of the hyperbranched NCs increased dramatically in response to μM concentrations of dithiothreitol (DTT).

Introduction

Mn^{2+}-doped semiconductors are widely used in many photo- and electroluminescent applications.[1,2] The availability of luminescent colloidal nanocrystals (NCs) of these materials expanded their use to bioimaging and sensing,[3–5] and solar energy,[6–8] among other applications.[9,10] The nature of the Mn^{2+} dopants can provide a probe of local environment, elucidating NC structural information *via* their optical and magnetic properties.[11–14] Applications involving Mn^{2+} phosphorescence involve doping of wide bandgap semiconductors.[15] The fixed $^4T_1$ energy level of the Mn^{2+} provides a trap for energy absorbed by the NC. This energy is released radiatively as an orange luminescence. This is only observed when the conduction band energy level is above the energy of the Mn^{2+} $^4T_1$, and thus frequently the zinc chalcogenides are employed as host materials.[3,13,15–18]

Dichalcogenides, namely diorganyl dichalcogenides, have recently been revived as synthons in colloidal NC syntheses.[19–22] They are touted for their ability to provide access to unfavourable crystal phases,[19] resulting in a myriad of NC shapes, compositions, and properties.[20–22] Their reactivity can be tuned by changing the organic substituents, allowing formation of quantum dots, tetrapods, nanorods, and other asymmetric, hyperbranched NCs from nearly identical reaction conditions.[20]

Hyperbranched and asymmetric semiconductor nanocrystals have large surface-area-to-volume ratios often resulting in a large number of surface defects.[23,24] Both of these characteristics garner interest for use of these NCs for selective, efficient catalysis,[25] gas adsorption and sensing,[26] and defect-related luminescence.[27]

Luminescent Mn^{2+}-doped chalcogenide NCs are readily synthesized using colloidal methods.[15,16] Protocols using binary clusters,[28,29] multi-step shell additions,[12] and post-synthetic diffusion[30] have been established. Each method provides advantages and disadvantages, such that the synthetic method can be chosen depending on the application requirements. Overall, these methods have multiple steps often involving reactive, expensive precursors, and the products of these syntheses have been limited in scope. This is ascribed to the difficulty in doping transition metal ions into anisotropic NCs.[31,32] Although there are numerous reports of emissive Mn^{2+}-doped spherical NCs and even nanorods,[33–39] there are only two reports of luminescent asymmetric Mn^{2+}-doped NCs.[32,40] In the detailed work of Wu & Warner, luminescent Mn^{2+}-doped ZnSe NCs were synthesized with spherical and pod-like structures. The branching is ascribed to polymorphism, resulting in tetrapods, with average sizes of 15 nm.[24,40] A sophisticated, successful effort to obtain asymmetric luminescent Mn^{2+}-doped NCs was presented by Yao *et al.*

Department of Chemistry, 213 Chemistry and Biochemistry Building, Kansas State University, Manhattan, KS 66506, USA. E-mail: mclaurin@k-state.edu

† Electronic supplementary information (ESI) available: Additional TEM images and luminescence spectra. See DOI: 10.1039/c6tc01207h

in which a one-pot synthesis generated elongated doped NCs exhibiting Mn^{2+} emission. The worm-like shapes and defects support an oriented-attachment-type growth of these 4–10 nm long particles.[32,41,42]

Here we report the first example, to the best of our knowledge, of luminescent Mn^{2+}-doped hyperbranched NCs. Zinc chalcogenides were chosen to exploit the characteristic luminescence observed from the Mn^{2+} $^4T_1 \rightarrow {}^6A_1$ transition. Changing the dichalcogenide precursors resulted in different morphologies, with compositions varying with precursor ratios. An electron paramagnetic resonance (EPR) signal is observed for the NCs, providing additional evidence for doping and information about the NC structure. This simple procedure provides a new synthetic method for successful incorporation of Mn^{2+} in wide bandgap $ZnSe_{1-x}S_x$ semiconductor NCs using dichalcogenide precursors. The incorporation of a radiative defect allows luminescence to be observed from these materials.

Experimental section

Materials

All the following chemicals are commercially available and were used without further purification; manganese(II) acetate tetrahydrate ($Mn(OAc)_2{\cdot}4H_2O$, ≥99%), manganese(II) chloride tetrahydrate ($MnCl_2{\cdot}4H_2O$, 99.99%), oleylamine (OLA, ≥98%), stearic acid (SA, ≥95%), dodecane thiol (DDT, ≥98%), selenium (≥99.5%), tetramethylammonium chloride (NMe_4Cl, ≥98%), triethylamine (TEA), cyclohexane, toluene, water, phosphate buffered saline (PBS), and chloroform from Aldrich, diphenyl diselenide (Ph_2Se_2, 99%), dimethyl disulfide (Me_2S_2, 99%), phenylselenol (PhSeH, 98%), and methanol (MeOH) from Acros, zinc nitrate hexahydrate ($Zn(NO_3)_2{\cdot}6H_2O$) from J. T. Baker, acetone, dithiothreitol (DTT), and L-lysine from Fisher, and zinc undecylenate ($Zn(Un)_2$) from Gelest.

Preparation of manganese stearate ($Mn(St)_2$)

A mixture of $Mn(OAc)_2{\cdot}4H_2O$ (1.000 g, 4.08 mmol) and stearic acid (5.226 g, 18.37 mmol) were degassed under vacuum at 100 °C and then under inert atmosphere, the temperature was increased to 180 °C and held for 20 minutes. After cooling the reaction mixture to 100 °C, the reaction mixture was degassed for another 60 minutes. The flask was cooled down to room temperature and a white solid was obtained.

Hyperbranched Mn^{2+}:ZnSe (1)

In a three neck flask $Mn(St)_2$ (~0.003 g, 5 μmol), zinc undecylenate (0.0865 g, 0.200 mmol), Ph_2Se_2 (0.1000 g, 0.32 mmol) and OLA (5.00 g, 18.7 mmol) were degassed at 100 °C for 90 minutes and then under nitrogen atmosphere, the temperature was increased to 280 °C and held for 10–60 minutes. Next, the heating mantle was removed, and the reaction mixture was cooled down to 65 °C immediately using a water bath. Finally, 2 ml of toluene was added to the reaction mixture followed by 5 ml of methanol. The particles were separated by centrifugation, resuspended in toluene, and precipitated with methanol again. The final sample was dispersed in cyclohexane. Mn^{2+}:ZnSe NCs were also synthesized using $Mn(OAc)_2{\cdot}4H_2O$ and $MnCl_2{\cdot}4H_2O$ under analogous conditions.

Mn^{2+}:$ZnSe_{1-x}S_x$ (2–5)

Samples were prepared using a procedure similar to that for **1**, but with mixtures of Ph_2Se_2 and Me_2S_2 or Ph_2S_2. The total amount of dichalcogenide was kept near ~0.33 mmol. Ratios of $Ph_2Se_2 : R_2S_2$ were approximately 3 : 1 (**2**), 1 : 1 (**3a**), 4 : 5 (**3b**), and 1 : 3 (**4**). In the case of Mn^{2+}:ZnS (**5**), Me_2S_2 (31 μl, 0.35 mmol) was used instead of Ph_2Se_2 and the reaction was carried out at 300 °C. Because of the lower boiling point of Me_2S_2, it must be injected into the reaction mixture after the degassing step.

$[NMe_4]_2[Zn_4(SePh)_{10}]$

The cluster precursor was prepared by adapting previous methods.[43,44] Three separate solutions were prepared and degassed for 30–60 minutes by bubbling with N_2: (1) $Zn(NO_3)_2{\cdot}6H_2O$ (7.318 g) in 35 ml MeOH, (2) Me_4NCl (4.42 g) in 20 ml MeOH, and (3) TEA (9.5 g) in 20 ml MeOH. Under a N_2 overpressure, PhSeH (10 g) was added to solution 3, followed by stirring for 20 minutes. Solution 1 was then transferred to solution 3 dropwise *via* cannula, forming a cloudy solution. Next, solution 2 was cannula transferred to solution 3 over a period of 10–30 min, followed by cooling in an ice bath for 30 minutes. The solid was then filtered and rinsed thoroughly with MeOH and toluene, yielding a white powder.

Mn^{2+}:ZnSe (6)

Unbranched Mn^{2+}:ZnSe NCs were synthesized by adapting previously described methods.[28,44] Briefly, OLA (10 g) and $MnCl_2{\cdot}4H_2O$ (0.0012 g, 6.1 μmol) were combined in a flask and degassed at 100 °C under vacuum for 120 minutes. After cooling below 80 °C, the cluster precursor (0.2 g, 0.073 mmol) and Se (0.0108 g, 0.137 mmol) were added under N_2 overpressure. After briefly degassing the solution under vacuum at 100 °C, the reaction was heated to 280 °C under N_2 and the NCs were grown at this temperature for 15 minutes. After cooling below 80 °C, the NCs were isolated by precipitation and resuspension with MeOH and toluene, respectively.

Water-soluble hyperbranched Mn^{2+}:ZnSe

A simple ligand-exchange method was used to suspend the NCs in aqueous solution. Previously prepared NCs were dispersed in toluene, precipitated out using methanol, and isolated by centrifugation. This procedure was repeated 3–4 times. Then, the NCs were dispersed in chloroform, precipitated out after adding acetone, and isolated by centrifugation. This process was repeated twice. Next, the NCs were dispersed in chloroform (4 ml) and an aqueous solution of L-lysine (0.03 g in 10 ml water) was added to it and stirred vigorously overnight. Then, the NCs were precipitated out by centrifugation and dispersed in PBS.

Thiol titrations

Thiol titration experiments were performed using a PTI Quanta Master 400 fluorometer. The samples were prepared in a 10 mm septum-sealed screw-top cuvette (Starna Cells, Inc.) with a stir bar and were diluted to have absorbance ~0.3 at 350 nm. A syringe pump (New Era Pump Systems, Inc.) was used for the titration with injection of thiol *via* a syringe with NanoTight™ adapters (Idex Health & Science, LLC) and 250 μm diameter flexible fused silica capillary tubing (Polymicro Technologies) which was inserted through the cuvette septum. While stirring, spectra were taken at intervals of 2–30 minutes, depending on sample brightness and sensitivity. Titrations were done until sample saturation.

Physical measurements

In this study a Cary 500 UV-Vis-NIR spectrophotometer was used for recording UV-Vis absorption spectra. A PTI Quanta Master 400 fluorometer was used to record photoluminescence and photoluminescence excitation spectra. For transmission electron microscopy (TEM) analysis, a drop of sample was dried on a copper grid. TEM images were recorded using a FEI Tecnai G2 Spirit BioTWIN microscope. The EPR spectrum was recorded using a Bruker EMXplus X-band EPR spectrometer. Powder X-ray diffraction (XRD) patterns were recorded using a PANalytical Empyrean multi-purpose X-ray diffractometer.

Results and discussion

Formation of Mn^{2+}:$ZnSe_{1-x}S_x$ nanocrystals

This procedure is related to the synthesis of Mn^{2+}-doped II–VI NCs using a tetramer ($[Zn_4(EPh)_{10}]^{2-}$) or decamer ($[Zn_{10}Se_4(EPh)_{16}]^{4-}$) cluster precursor. Both methods nucleate and grow NCs in a single, heat-up step and the cluster contains organyl chalcogenide ligands (phenylthiols and phenylselenols) similar to the dichalcogenides used here.[28,29] The most widely used cluster has E = S, likely because of the high cost of the selenol precursor (*vs.* thiol). However, NCs synthesized with this precursor are known to contain sulphur impurities.[29] The key advantages of the dichalcogenide-doping method presented here are the simplified procedure, as preparation of cluster precursor(s) is not required, and the air-stable diselenide precursor is substantially less expensive than the phenylselenol precursor required for metal-selenide cluster synthesis.

The procedure used to obtain the NCs is shown in Fig. 1. Generally, a Zn^{2+} precursor (zinc undecylenate), Mn^{2+} precursor (manganese stearate), and dichalcogenide(s) are combined in a coordinating solvent (oleylamine). After heating at 280 °C in an inert atmosphere for 10–60 minutes, NCs form. The exception was for Mn^{2+}:ZnS (**5**), which required 300 °C to obtain a significant quantity of NCs. The NCs are isolated by precipitation and resuspension in organic solvent followed by characterization to determine NC photophysical and magnetic properties, and structures.

Initially, NCs were synthesized using only the Ph_2Se_2 dichalcogenide precursor (**1**). These NCs exhibited absorption and PL

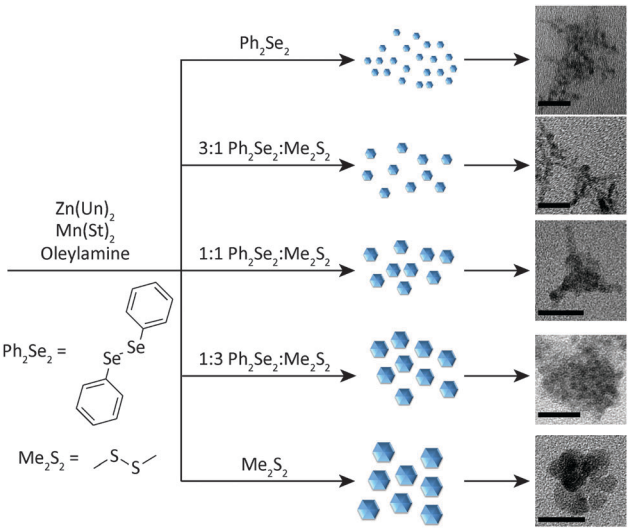

Fig. 1 General synthetic scheme for formation of Mn^{2+}-doped $ZnSe_{1-x}S_x$ NCs. In the reaction, zinc undecylenate, $Zn(Un)_2$, manganese stearate, $Mn(St)_2$, and a mixture of diphenyl diselenide and dimethyl disulphide (or diphenyl disulphide) are combined and heated to reaction temperature in an alkylamine under an inert atmosphere. Depending on the ratio of diselenide to disulphide, NCs of different shapes and sizes are obtained. Images of samples **1–5** are shown. Scale bars are 20 nm.

spectra characteristic of Mn^{2+}:ZnSe NCs (Fig. 2, black line). The absorption feature near 390 nm indicates formation of the ZnSe host NCs. The PL spectrum has a peak centred at 586 nm, indicative of Mn^{2+} luminescence. The rapid transfer of energy from the NC to the Mn^{2+} efficiently competes with excitonic recombination, and no blue ZnSe emission is observed. Subsequent reactions combined the Ph_2Se_2 precursor with a disulphide precursor, to form Mn^{2+}:$ZnSe_{1-x}S_x$ NCs of different shapes. Two disulphide precursors were used: Ph_2S_2 and Me_2S_2. Starting ratios of diselenide to disulphide were varied from 1 : 0 (**1**), 3 : 1 (**2**), 1 : 1 (**3**), 1 : 3 (**4**), and 0 : 1 (**5**). The first absorption feature of the NCs blue-shifted from that of **1**, indicating likely sulphur incorporation, with a systematic decrease in wavelength with increasing Me_2S_2.

Comparing absorption and emission spectra for the Me_2S_2 and Ph_2S_2 samples with similar ratios (**3a** and **3b**), yields insight

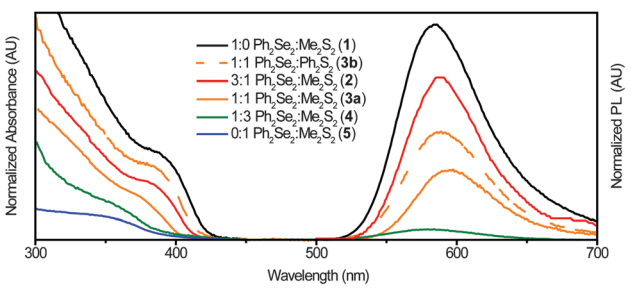

Fig. 2 Absorption (left) and PL (right) spectra of Mn^{2+}:$ZnSe_{1-x}S_x$ NCs with varying dichalcogenide precursor ratios. The NC first absorption peak shifts from ~390 nm for Ph_2Se_2 alone (**1**) to a broad feature at ~340 nm for Me_2S_2 alone (**5**). The PL peak red-shifts from 586 nm to 589 nm with increasing S. For **4**, very little luminescence was detected and for **5** no luminescence was detected.

into the effect of disulphide precursor on the resulting product. Although similar ratios were used, the absorption of **3a** is noticeably blue-shifted from that of **3b**, indicating decreased reactivity of Ph_2S_2 *vs.* Me_2S_2, as reported previously.[20] These NCs (**3b**) exhibit a PL peak at 588 nm, slightly red-shifted from the PL peak of **1** at 586 nm. For the other NC samples, the PL peaks red-shifted to 589 nm with increasing disulphide (**2**, **3a**). The PL intensity decreased with larger Me_2S_2 amounts, such that only a broad, very weak peak was observed for **4** and none was detectable in the Me_2S_2 only sample (**5**). To confirm the orange PL associated with Mn^{2+} was coming from the NCs, photoluminescence excitation (PLE) spectra were taken. The resulting spectra (Fig. S1, ESI†) exhibit the characteristic first absorption feature of the NCs with a continued increase at higher energies.

Morphology and structure of Mn^{2+}:$ZnSe_{1-x}S_x$ nanocrystals

The key to changing the NC shape and degree of branching is the ratio of diselenide to disulphide precursor. Fig. 3 shows TEM images of NCs prepared with varying ratios of diselenide and disulphide. As the amount of disulphide increases, the particles go from branched networks to rounded, linked platelets. Comparing **3a** and **3b** (Fig. 3d and b) further illustrates the effect of disulphide on the reaction. The TEM image of **3b** more closely resembles that of **1** (Fig. 3a), exhibiting significant branching. This branching appears to stem not only from the centre of a particle, but also from the outward reaching NC arms (Fig. S2–S5, ESI†). The appearance of isolated particles (shown in Fig. 3 insets) within the samples suggests oriented attachment may be occurring as well, creating highly branched networks.[41,45,46] This will be discussed further in the discussion of the formation mechanism. TEM images of **2** and **3a** (Fig. 3c and d) also exhibit networks of hyperbranched particles. Although these networks are complex, the insets provide key details about the smaller, branched particles forming the larger networks. For both **2** and **3a**, smaller particles with more rounded, thicker arms are observed. These characteristics are passed on to the networks that form. Further increases in the S : Se ratio show formation of larger, rounder particles, followed by oriented attachment to form large, spherical clusters of NCs (Fig. 3e and Fig. S6, ESI†). When only Me_2S_2 is used as the dichalcogenide precursor, large, round platelets form and link together, generating round clusters of these NCs (Fig. 3f and Fig. S7, ESI†). Syntheses of Mn^{2+}:ZnSe with other Mn^{2+} precursors produced similar hyperbranched NCs (Fig. S8, ESI†).

Additional structural information about the NCs was obtained from XRD. The diffraction patterns in Fig. 4a exhibit a zinc-blende pattern, with highly broadened peaks due to the small domain size of the NCs. With increasing disulphide precursor, the peaks shift to larger angles, characteristic of a transition from ZnSe to ZnS. Peak positions indicate larger sulphur content for sample **3a** than **3b**, providing additional evidence for the low reactivity of Ph_2S_2 *vs.* Me_2S_2. Ultimately, the peak shifts for **3a** are small relative to what is expected for a 1 : 1 ratio of S : Se in the NCs, indicating a decreased reactivity for Me_2S_2 (*vs.* Ph_2Se_2). No Mn diffraction peaks are observed, indicating successful doping of Mn^{2+} ions into the NCs.[47]

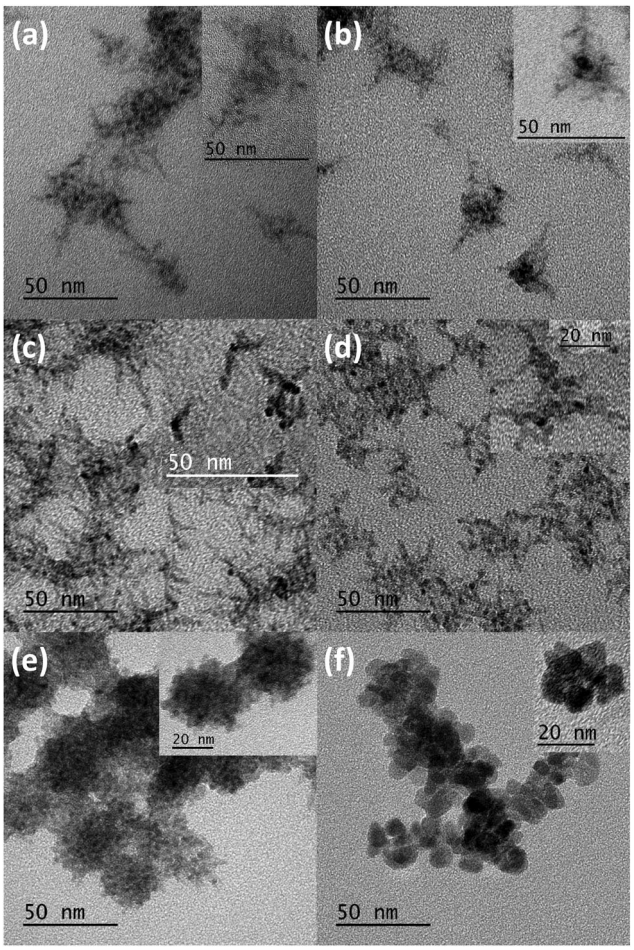

Fig. 3 TEM images of (a) **1**, (b) **3b**, (c) **2**, (d) **3a**, (e) **4**, and (f) **5**. Large image scale bars are 50 nm. Inset image scale bars are 50 nm for a–c and 20 nm for d–f. Highly branched structures at low S : Se ratios transition to more spherical samples at higher S : Se ratios. Insets highlight particles that are linking together, likely through oriented attachment, to form larger networks and aggregates of the NCs. The shape, size, and structure of these particles is reflected in the larger structure of the resulting nanomaterial.

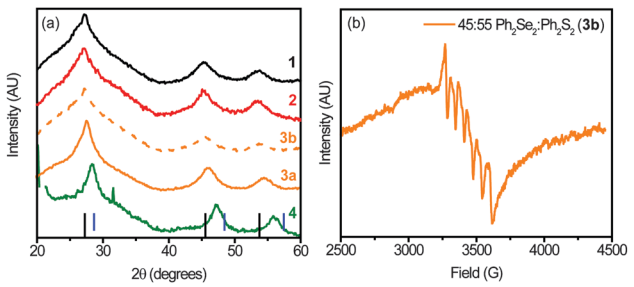

Fig. 4 (a) XRD patterns of samples **1**, **2**, **3a**, **3b**, and **4**. The patterns indicate zinc-blend structure and the broadness of the peaks indicates small NC diameters or domains. As the amount of S increases, the peaks shift to larger angles. The black lines at the bottom of the figure represent the positions of bulk ZnSe and the blue lines represent those of bulk ZnS. (b) EPR spectrum of **3b** showing a splitting pattern with 6 peaks and a hyperfine coupling constant of 66.2 G.

Additional evidence of successful Mn^{2+} doping into these NCs is provided by EPR. The EPR spectrum of **3b** is shown in Fig. 4b. The 6-peak hyperfine structure characteristic of Mn^{2+} is observed. In addition, a coupling constant of 66.2 G is estimated, consistent with values found for ZnSe (66.1 G)[16] and ZnS (68.4 G).[48] The estimated value is substantially smaller than that of surface Mn^{2+} ($\sim$90 G),[13,14,49] further affirming Mn^{2+} incorporation.

Possible formation mechanisms

The dichalcogenides are known to produce nanomaterials with a variety of morphologies.[20–22] Vela and co-workers presented an elegant study in which differences in dichalcogenide bond dissociation energies were correlated with changes in particle size and shape, and found diselenide precursors reacted more quickly than analogous disulphides.[20] Although the systems studied differ from those presented here (they used Cd^{2+}, different ligands, lower temperatures, and hot-injection), the results can help explain the observed trend in particle size and shape.

The formation of the NCs shown in Fig. 3 can be explained in terms of the precursor reactivity of the disulphide *vs.* Ph_2Se_2. Thus, for the faster reacting Ph_2Se_2-containing reactions, the initially formed particles are relatively small in diameter, and begin branching and attaching to form the more complex networks seen in Fig. 3a–d. This behaviour has been attributed to the introduction of more branching angles due to twinning defects that occur in samples with more rapid growth.[23] When larger amounts of the less reactive Me_2S_2 are present, larger particles form due to slow growth, which leads to less branching. Over time, these particles begin to link together, likely *via* oriented attachment.[24,41] At final reaction times, the reaction product is a network of these linked particles. A cartoon of this possible mechanism is shown in Fig. 1, in which with less Me_2S_2, smaller particles form and aggregate, forming more highly-branched, polycrystalline networks. With more Me_2S_2, larger NCs form before coming together to form rounded aggregates of platelets. Thus, there does not appear to be an additional ripening process occurring during the attachment process, and the final sample is characteristic of the initial NC size, as observed for similar systems.[20]

Application of NCs for thiol sensing

As mentioned in the introduction, an advantage of branched NCs is their large surface area, which makes them useful for applications in sensing, among others.[25–27] Thiols are known to influence processes in biology and play key roles in nano-devices.[50–54] To explore the potential application of these highly branched Mn^{2+}-doped NCs, the luminescence enhancement in the presence of thiol was studied.

DDT was used as a model thiol and Fig. 5a depicts the PL enhancement observed when small amounts of DDT are added to a solution of **3b**. The Mn^{2+} PL increases, until eventually saturating at a concentration of $\sim$70 mM, as shown in Fig. 5b. Similar, less-sensitive behaviour is observed for the less branched NCs (**2**) and NCs with no branching (**6**). This change in sensitivity could be due to the large number of NC defects, which decrease in the order: hyperbranched > branched > unbranched.

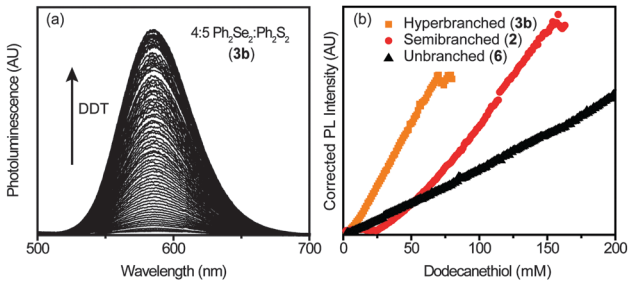

Fig. 5 (a) Steady-state PL of **3b** in the presence of dodecanethiol (DDT). Increasing the amount of thiol leads to a concomitant increase in Mn^{2+} PL from the NCs. (b) Scatter plot of the Mn^{2+} PL intensity *vs.* [DDT] for NC samples with different degrees of branching. The more branched **3b** NCs show the steepest increase in PL intensity with thiol. NCs with less (**2**) and no (**6**) branching show decreasing sensitivity to thiol, with smaller increases in slope.

Addition of DDT may passivate these defects, providing more efficient energy transfer to the Mn^{2+}-dopants, and a brighter Mn^{2+} luminescence.[55–57]

To demonstrate the utility of these NCs for biological sensing, the NCs were transferred to aqueous solution. After transfer, the Mn^{2+} luminescence of the NCs decreased, but not significantly. The NCs illuminated by a UV lamp before and after water-solubilization are shown in Fig. 6a. Once in aqueous solution, the NCs were titrated with dithiothreitol (DTT), with a corresponding increase in PL (Fig. 6b). DTT is key in the study of biological functions such as protein unfolding, signal transduction, and as a redox mediator.[58–61] Here, it acts as a reductant, enhancing the NC PL at concentrations from 0 to $\sim$40 μM before decreasing again at concentrations $>\sim$60 μM (Fig. 6c). The sensitivity of the NCs to DTT is linear within this range, with an analytical sensitivity of 2.9 μM and a detection limit of 1.0 μM.

This simple sensor exhibits a large, linear increase in luminescence with thiol, highlighting the advantages of these NCs as sensors. In organic solvent, differences in sensitivity (ΔPL *vs.* ΔDDT) vary with branching, although additional study is required to explore the complex interplay of structure, branching, defect formation, and dopant incorporation, which all likely play a

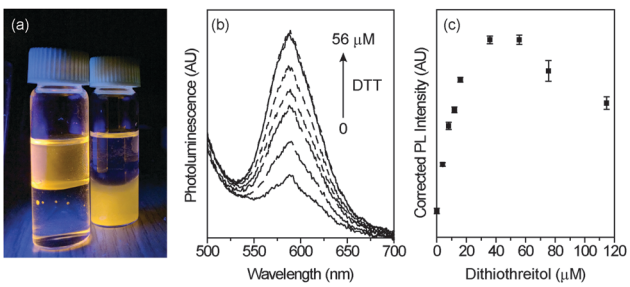

Fig. 6 (a) Photograph of Mn^{2+}-doped hyperbranched NCs illuminated by a UV lamp in aqueous solution and in chloroform. (b) Steady-state PL of hyperbranched Mn^{2+}–ZnSe NCs in PBS with addition of a dithiothreitol (DTT) solution. As the concentration of DTT increases from 0 to 56 μM, the Mn^{2+} PL increases. (c) Scatter plot of the Mn^{2+} PL intensity *vs.* [DTT] exhibiting a linear increase in luminescence in the μM range before decreasing in intensity at concentrations >60 μM.

role in the luminescence response. In aqueous medium, enhancement of PL by DTT is linear at low concentrations, with high sensitivities. The mechanism of PL increase is likely related to passivation of surface traps, providing a pathway for enhanced sensitivity to biological thiols through the increase in surface defects present in these hyperbranched Mn^{2+}-doped materials.

Conclusions

A new synthetic method for obtaining doped $ZnSe_{1-x}S_x$ NCs yields luminescent NCs of a variety of structures. Variations in dichalcogenide precursor can be used to tune the NC size and shape. Knowing these trends in reactivity, syntheses can be designed to obtain NCs of desired size, shape, and dopant incorporation. This method provides access to luminescent materials that are not usually emissive due to high defect levels. The resulting emissive, hyperbranched materials decrease losses in PL due to defects by employing Mn^{2+} as a luminescent trap. These NCs can be used as turn-on thiol sensors, with sensitivity varying with branching in organic solution. A similar response is observed in aqueous solution, with a large increase in PL at low thiol levels. This synthetic procedure is extendable to other NC systems synthesized using dichalcogenides and other dopants, providing a new pathway to luminescent, hyperbranched materials.

Acknowledgements

This research was supported by Kansas State University. A KS-USRG provided financial support. TEM images were obtained through the Nanotechnology Innovation Centre of Kansas State (NICKS). The authors thank C. Gura for assistance with XRD (Department of Geology) and J. Douglas for assistance with EPR (University of Kansas).

References

1 T. Jüstel, in *Luminescence*, ed. C. Ronda, Wiley-VCH Verlag GmbH & Co. KGaA, Weinheim, Germany, 2007, ch. 3, pp. 61–73.
2 G. Blasse and B. C. Grabmaier, *Luminescent Materials*, Springer, Berlin Heidelberg, 1994, ch. 6, pp. 108–133.
3 R. Thakar, Y. Chen and P. T. Snee, *Nano Lett.*, 2007, **7**, 3429–3432.
4 S. Santra and D. Dutta, in *Nanoparticles in Biomedical Imaging*, ed. J. W. M. Bulte and M. M. J. Modo, Springer, New York, 2008, ch. 22, vol. 3, pp. 463–485.
5 P. Wu and X.-P. Yan, *Chem. Soc. Rev.*, 2013, **42**, 5489–5521.
6 P. K. Santra and P. V. Kamat, *J. Am. Chem. Soc.*, 2012, **134**, 2508–2511.
7 T. Debnath, P. Maity, S. Maiti and H. N. Ghosh, *J. Phys. Chem. Lett.*, 2014, **5**, 2836–2842.
8 J. Tian, L. Lv, C. Fei, Y. Wang, X. Liu and G. Cao, *J. Mater. Chem. A*, 2014, **2**, 19653–19659.
9 Z. Hu, S. Xu, X. Xu, Z. Wang, Z. Wang, C. Wang and Y. Cui, *Sci. Rep.*, 2015, **5**, 14817.
10 H.-J. Kim, H.-D. Lee, C. S. S. P. Kumar, S. S. Rao, S.-H. Chung and D. Punnoose, *New J. Chem.*, 2015, **39**, 4805–4813.
11 S. Ithurria, P. Guyot-Sionnest, B. Mahler and B. Dubertret, *Phys. Rev. Lett.*, 2007, **99**, 265501.
12 Y. Yang, O. Chen, A. Angerhofer and Y. C. Cao, *J. Am. Chem. Soc.*, 2008, **130**, 15649–15661.
13 S. Acharya, D. D. Sarma, N. R. Jana and N. Pradhan, *J. Phys. Chem. Lett.*, 2010, **1**, 485–488.
14 W. Zheng, Z. Wang, J. Wright, B. Goundie, N. S. Dalal, R. W. Meulenberg and G. F. Strouse, *J. Phys. Chem. C*, 2011, **115**, 23305–23314.
15 R. Beaulac, S. T. Ochsenbein and D. R. Gamelin, in *Nanocrystal Quantum Dots*, ed. V. I. Klimov, CRC Press, Boca Raton, FL, USA, 2nd edn, 2010, ch. 11, pp. 397–453.
16 D. J. Norris, N. Yao, F. T. Charnock and T. A. Kennedy, *Nano Lett.*, 2001, **1**, 3–7.
17 R. N. Bhargava, D. Gallagher, X. Hong and A. Nurmikko, *Phys. Rev. Lett.*, 1994, **72**, 416–419.
18 J. H. Yu, S.-H. Kwon, Z. Petrášek, O. K. Park, S. W. Jun, K. Shin, M. Choi, Y. I. Park, K. Park, H. B. Na, N. Lee, D. W. Lee, J. H. Kim, P. Schwille and T. Hyeon, *Nat. Mater.*, 2013, **12**, 359–366.
19 M. E. Norako, M. A. Franzman and R. L. Brutchey, *Chem. Mater.*, 2009, **21**, 4299–4304.
20 Y. Guo, S. R. Alvarado, J. D. Barclay and J. Vela, *ACS Nano*, 2013, **7**, 3616–3626.
21 J. Wang, A. Singh, P. Liu, S. Singh, C. Coughlan, Y. Guo and K. M. Ryan, *J. Am. Chem. Soc.*, 2013, **135**, 7835–7838.
22 R. L. Brutchey, *Acc. Chem. Res.*, 2015, **48**, 2918–2926.
23 A. G. Kanaras, C. Sönnichsen, H. Liu and A. P. Alivisatos, *Nano Lett.*, 2005, **5**, 2164–2167.
24 H. Li, A. G. Kanaras and L. Manna, *Acc. Chem. Res.*, 2013, **46**, 1387–1396.
25 Z.-Y. Zhou, N. Tian, J.-T. Li, I. Broadwell and S.-G. Sun, *Chem. Soc. Rev.*, 2011, **40**, 4167–4185.
26 T.-D. Nguyen, C.-T. Dinh and T.-O. Do, *Chem. Commun.*, 2015, **51**, 624–635.
27 K. Nose, Y. Soma, T. Omata and S. Otsuka-Yao-Matsuo, *Chem. Mater.*, 2009, **21**, 2607–2613.
28 S. L. Cumberland, K. M. Hanif, A. Javier, G. A. Khitrov, G. F. Strouse, S. M. Woessner and C. S. Yun, *Chem. Mater.*, 2002, **14**, 1576–1584.
29 P. I. Archer, S. A. Santangelo and D. R. Gamelin, *J. Am. Chem. Soc.*, 2007, **129**, 9808–9818.
30 V. A. Vlaskin, C. J. Barrows, C. S. Erickson and D. R. Gamelin, *J. Am. Chem. Soc.*, 2013, **135**, 14380–14389.
31 J. H. Yu, X. Liu, K. E. Kweon, J. Joo, J. Park, K.-T. Ko, D. W. Lee, S. Shen, K. Tivakornsasithorn, J. S. Son, J.-H. Park, Y.-W. Kim, G. S. Hwang, M. Dobrowolska, J. K. Furdyna and T. Hyeon, *Nat. Mater.*, 2010, **9**, 47–53.
32 T. Yao, S. Kou, Y. Sun, Q. Zhao and J. Yang, *CrystEngComm*, 2012, **14**, 8440–8445.
33 J. D. Bryan and D. R. Gamelin, in *Prog. Inorg. Chem.*, ed. K. D. Karlin, John Wiley & Sons, Inc., Hoboken, NJ, USA, 2005, ch. 2, vol. 54, pp. 47–126.
34 S. W. Lu, B. I. Lee, Z. L. Wang, W. Tong, B. K. Wagner, W. Park and C. J. Summers, *J. Lumin.*, 2000, **92**, 73–78.

35 J. Y. Lee, D. S. Kim, J. H. Kang, S. W. Yoon, H. Lee and J. Park, *J. Phys. Chem. B*, 2006, **110**, 25869–25874.
36 P. T. K. Chin, J. W. Stouwdam and R. A. J. Janssen, *Nano Lett.*, 2009, **9**, 745–750.
37 M. Zhang, Y. Lu, J.-F. Chen, T.-K. Zhang, Y.-Y. Liu, Y. Yang, W.-T. Yao and S.-H. Yu, *Langmuir*, 2010, **26**, 12882–12889.
38 S. Acharya, S. Sarkar and N. Pradhan, *J. Phys. Chem. C*, 2013, **117**, 6006–6012.
39 C. Q. Jin, C. H. Ge, G. Xu, Y. X. Wei, Q. P. Ding, M. Zhu and H. B. Duan, *J. Alloys Compd.*, 2015, **648**, 481–487.
40 Y. A. Wu and J. H. Warner, *J. Mater. Chem.*, 2012, **22**, 417–424.
41 W. Lv, W. He, X. Wang, Y. Niu, H. Cao, J. H. Dickerson and Z. Wang, *Nanoscale*, 2014, **6**, 2531–2547.
42 X. Xue, R. L. Penn, E. R. Leite, F. Huang and Z. Lin, *CrystEngComm*, 2014, **16**, 1419–1429.
43 I. G. Dance, A. Choy and M. L. Scudder, *J. Am. Chem. Soc.*, 1984, **106**, 6285–6295.
44 V. A. Vlaskin, R. Beaulac and D. R. Gamelin, *Nano Lett.*, 2009, **9**, 4376–4382.
45 R. L. Penn and J. F. Banfield, *Science*, 1998, **281**, 969–971.
46 H. Zhang, R. L. Penn, Z. Lin and H. Cölfen, *CrystEngComm*, 2014, **16**, 1407–1408.
47 B. Yang, X. Shen, H. Zhang, Y. Cui and J. Zhang, *J. Phys. Chem. C*, 2013, **117**, 15829–15834.
48 B. J. Park, W. B. Im, W. J. Chung, H. S. Seo, J. T. Ahn and D. Y. Jeon, *J. Mater. Res.*, 2007, **22**, 2838–2844.
49 L. Zu, A. W. Wills, T. A. Kennedy, E. R. Glaser and D. J. Norris, *J. Phys. Chem. C*, 2010, **114**, 21969–21975.
50 Z. J. Donhauser, B. A. Mantooth, K. F. Kelly, L. A. Bumm, J. D. Monnell, J. J. Stapleton, D. W. Price, A. M. Rawlett, D. L. Allara, J. M. Tour and P. S. Weiss, *Science*, 2001, **292**, 2303–2307.
51 D. M. Townsend, K. D. Tew and H. Tapiero, *Biomed. Pharmacother.*, 2003, **57**, 145–155.
52 Q. Li and J. R. Lancaster, *Nitric Oxide-Biol. Chem.*, 2013, **35**, 21–34.
53 E. A. Weiss, *Acc. Chem. Res.*, 2013, **46**, 2607–2615.
54 L. Sun, Y. A. Diaz-Fernandez, T. A. Gschneidtner, F. Westerlund, S. Lara-Avila and K. Moth-Poulsen, *Chem. Soc. Rev.*, 2014, **43**, 7378–7411.
55 A. L. Weaver and D. R. Gamelin, *J. Am. Chem. Soc.*, 2012, **134**, 6819–6825.
56 J. D. Rinehart, A. L. Weaver and D. R. Gamelin, *J. Am. Chem. Soc.*, 2012, **134**, 16175–16177.
57 S. Sarkar, B. K. Patra, A. K. Guria and N. Pradhan, *J. Phys. Chem. Lett.*, 2013, **4**, 2084–2090.
58 R. E. Feeney, R. B. Yamasaki and K. F. Geoghegan, in *Modification of Proteins*, ed. R. E. Feeney and J. R. Whitaker, American Chemical Society, Washington, DC, USA, 1982, ch. 1, vol. 198, pp. 3–55.
59 S. García-Santamarina, S. Boronat and E. Hidalgo, *Biochemistry*, 2014, **53**, 2560–2580.
60 W. W. Cleland, *Biochemistry*, 1964, **3**, 480–482.
61 R. P. Szajewski and G. M. Whitesides, *J. Am. Chem. Soc.*, 1980, **102**, 2011–2026.